https://dx.doi.org/10.1016/j.enggeo.2023.107398

An experimental study of stress-dependent water retention behaviour of two lateritic clays with different minerals

Seth, O. Tawiah, Charles, W.W. Ng, Chao, Zhou* (corresponding author)

Author's affiliation and address:

Name: Seth Tawiah Owusu

Title: MPhil Graduate

Affiliation: Department of Civil and Environmental Engineering, Hong Kong

University of Science and Technology, Hong Kong

Email: sotawiah@connect.ust.hk

Name: Charles Wang Wai Ng

Title: CLP Holdings Professor of Sustainability

Affiliation: Department of Civil and Environmental Engineering, Hong Kong

University of Science and Technology, Hong Kong

Email: cecwwng@ust.hk

Name: Chao Zhou*

Title: Assistant Professor

Affiliation: Department of Civil and Environmental Engineering, The Hong Kong

Polytechnic University, Hung Hom, Hong Kong

Email: c.zhou@polyu.edu.hk

Abstract

Lateritic soils are associated with high content of sesquioxides which enhance the agglomeration of fine particles. The formation of aggregates can induce significant changes in the pore size distribution (PSD) and consequently affect the hydro-mechanical behaviour of lateritic soils. The influence of mineral types on the extent of aggregation and the stress-dependent water retention behaviour of lateritic clays is not well understood. In this study, the stress-dependent water retention curves (SDSWRCs) of a compacted lateritic sandy fat clay with halloysite (i.e., GLH) obtained from Ghana were measured at different net vertical stresses using an improved stress-controlled pressure plate apparatus. The results are then compared with those of another lateritic sandy lean clay with goethite (NLG) obtained from Nigeria. Additionally, scanning electron microscopy (SEM) and Brunauer-Emmett-Teller (BET) were employed to examine the microstructure associated with these soils. The experimental results show that GLH has a higher ability to retain water than NLG at any given suction, even though the former has a higher void ratio than the latter prior to the drying-wetting cycle. This is because the presence of relatively small aggregates and small-size macropores in the GLH as revealed by SEM images and BET results. On the other hand, the water retention capacity of both soils reduces with elevated stress levels, except at net vertical stress of 120 kPa for the GLH, with a corresponding decrease in rate of desaturation. Furthermore, the overall increase in the size of hysteresis loop measured is 4 times more lager for the NLG (i.e., 200%) than the GLH (i.e., 47%) in the stress and suction range considered, contrary to the decreasing trends commonly reported in literature. It was found that the sizes of aggregates in GLH reduced ('finer soil') as stress level increased and caused more water to be retained. Conversely to GLH, the aggregate size remained unchanged for the NLG, as revealed by aggregate size analysis. This is mainly because of the differences in the strengths provided by the unique minerals in

the two soils (i.e., halloysite for GLH and goethite for NLG) to the aggregates, due to the different parent rocks from which the soils were formed.

Keywords: Lateritic soil, water retention curve, unsaturated soil, aggregation, goethite mineral, halloysite mineral.

Introduction

The soil water retention curve (SWRC) is an important hydraulic property of unsaturated soil needed for analysing various coupled seepage and stability of earth structures such as slopes and embankments (Ng et al., 2020). It is generally reported in the literature that basic properties of soils, such as particle size distribution is adequate enough to describe the SWRC (Fredlund *et al*, 1997; Aubertin *et al*., 2003; Craig *et al*., 2014a; Ng et al., 2022). Particle size distribution, however, can be altered significantly due to chemical and mineralogical composition (Airey *et al*., 2012; Otalvaro *et al*., 2016; Ng et al., 2019). This is mainly because of the aggregation and (or) bonding of the fine content (e.g. Otalvaro *et al*., 2016). Moreover, the types of secondary minerals present also influence the response to compression of the resulting aggregates in the soil sample (Ng *et al*., 2019). Consequently, although the aggregates (or grains) can be arranged in many configurations that result in the same void ratio, pore structures, including pore size distributions, pore shapes, and pore orientations, are almost always different (Penumadu & Dean, 2000; Sivakumar & Wheeler, 2000; Koliji *et al*., 2010). Different responses of aggregates in soil samples during compaction (or compression) thus implies different initial compaction-induced structure. These changes would highly affect their hydro-mechanical behaviour (Zhou & Ng, 2014). Ng & Pang (2000a) found that water retention of unsaturated soil is strongly dependent on stress levels and has profound effects on slope stability analysis. Ignoring the effects of SDSWRC on slope stability analysis can lead to unsafe design (Ng & Pang, 2000b). This is because the application of stress affects both the soil density (or void ratio) and pore size distribution, as revealed in mercury intrusion porosimetry (MIP) test conducted by Thom *et al*. (2007) and Burton *et al*. (2014).

The relationship between soil structure, pore size distribution, and micro-aggregation of clay particles for lateritic soils has been studied (Miguel & Vilar, 2009; Otalvaro *et al*., 2016). The micro-aggregation associated with the soil structure of lateritic soils is well

recognised to be caused by the content of secondary oxides of iron and aluminium (Sunil & Krishnappa, 2012; Zhang *et al*., 2016; Ng *et al*., 2019). Nevertheless, how the resulting aggregates are affected by the presence of different types of minerals and how that will influence their geotechnical properties such as stress-dependent soil water retention curves (SDSWCs) are not studied.

There is a need therefore to study the influence of the variability in mineral type on the stability of the aggregation caused by sesquioxide contents and how their SDSWRCs and the associated hydraulic hysteresis are affected. In this study, the SDSWRCs of Ghana lateritic samples (i.e., GLH) is investigated. The results are compared with other data on Nigeria lateritic samples (i.e., NLG) (Ng et al., 2019), which has different mineral constituent but was tested following the same net vertical stress and suction path. Halloysite and goethite were unique minerals to GLH and NLG respectively, aside from the common minerals present in both soils.

Testing material and specimen preparation

Laterites and lateritic soils constitute about 8% of the soil on global earth surface (FAO 1989). The distribution of laterites and lateritic soils around the globe is illustrated in Figure 1 (after CIRIA, 1995). The basic properties of the soils considered in this study, including the lateritic soils sampled from Ghana (i.e., GLH) and Nigeria (i.e., NLG), are shown in Table 1. According to the unified soil classification system (ASTM, 2011), the GLH and NLG were classified as sandy fat clay (CH) and sandy lean clay (CL) respectively. The GLH test samples were compacted to 89% of Proctor maximum (or relative compaction *R.C.*) (1.377Mg/m^3) at 19.5% at dry-side of optimum moisture content (OMC).

Figure 2 depicts the PSD for the dry and wet sieving determined for the studied soils following BS1377 (1990). The figure reveals that the ‘particle size’ of GLH and NLG changed drastically from granular to fine materials upon wet sieve. The alteration in the PSD gives an

indication of the degree of aggregation in a soil sample (Otalvaro et al., 2016). This observation suggests that in these lateritic soils, many of the fine particles are strongly attached to form larger-size aggregates, which may not be remoulded during specimen preparation.

The XRF result shows that both soils contain significant amount of sesquioxides, nevertheless, the GLH contains a lower content of iron oxide than the NLG. More importantly, the XRD results show that the GLH and NLG contain a significant amount of halloysite and goethite minerals respectively, even though clay minerals such as quartz, hematite, and kaolinite are common to both soils. The main reason for the different minerals is likely because of the different parent rocks from which the soils are formed (Ampadu & Nocilla, 2017). The GLH and NLG were formed from phyllitic and granitic parent rocks, respectively. More details of the chemical and mineralogical properties of the two soils are summarised in Table 2. Their influence on the SDSWRC is discussed later.

All sample preparations were achieved following the same technique (Ng et al., 2016) to ensure the same void ratio at the initial state. Each specimen was compacted inside an oedometer ring of 70 mm in diameter and 19 mm in height, at a constant axial displacement rate of 1.0 mm/min.

Experimental program

A test program was designed to study the SDSWRC of recompacted GLH and compared the results with other data from the literature. Firstly, SDSWRCs were measured using the improved stress-controlled pressure plate apparatus (PPA) from a lower suction upto 400 kPa. Four specimens were tested under varying vertical stresses (i.e., 0, 40, 80 and 120 kPa) for the GLH. The selected stress conditions is to ensure that the objective of comparing test data with previous data could be achieved. Additionally, one more test at a higher stress

(200 kPa) was conducted to substantiate the observation reported in the previous work (Ng et al., 2019).

Testing apparatus and methods

The improved stress-controlled PPA utilised in this study is shown in Fig. 2. This apparatus allows continuous measurement of the drying and wetting SWRCs at various stresses. It also has a guard cell that prevents the possibility of eccentric loading of the specimen. More details on the apparatus are reported elsewhere (Ng et al. 2019).

Each specimen was saturated and then compressed. After that, suction was gradually increased upto 400 kPa and then decreased in steps to measure the drying and wetting curves, respectively. The end of each suction step was marked by the realization of equalization condition. Suction was assumed to be equalized when the inflow-outflow rate became less than or equal to $1.2 \times 10^{-12} m^3/s$. The criterion corresponds to a daily change of water content less than 0.05%. It took 3–12days for each suction stage.

SEM images were used to visually assess the degree of aggregation formed in these soils due to the presence of sesquioxides. The image analysis was performed on as-compacted samples that were prepared, following the freeze-drying technique (Delage & Pellerin, 1982; Zhang et al., 2018). Finally, the total pore volume (TPV) and specific surface area (SSA) was measured using the Brunauer-Emmett-Teller (BET) method (Maček et al., 2013).

Interpretation of experimental results

Stress-dependent SWRC of GLH

Figure 4a shows the SWRCs of GLH at various net vertical stresses. Ordinate represents degree of saturation while the abscissa presents suction. At suctions ranging from 0.1 to 50 kPa, the specimen subjected to 0 kPa net vertical stress retains more water than those under higher stresses. The figure depicts also that an increase in the net vertical stress resulted

in a decrease in the water retention capacity except at 120 kPa net vertical stress. In fact, the increase is so drastic that the water retention curves for the sample at 120 kPa stress shift above those of soil samples at 40 and 80 kPa net vertical stresses, except between 1 and about 3 kPa suction. Nevertheless, the curves still lie below that of zero net vertical stress at suction values lower than 30 kPa, whereas similar water retention capacity is observed between 30-60 kPa for both samples (i.e., 0 & 120 kPa). The observed behaviour suggests that for GLH the capacity to hold more water as suction is elevated increases drastically above a certain normal stress limit.

From the SWRCs, the desaturation and absorption rates estimated are summarized in Table 4 and is illustrated in Fig. 5. The data shows that the rate of desaturation increases with elevated stress levels but reduced at 120 kPa (Fig. 5a). A reduction in the rate of desaturation at higher stress levels is commonly reported in the literature (e.g. Salager *et al*., 2013; Ng *et al*., 2016). The increase in the rate of desaturation on the other hand, suggests that macropores become more continuous with rise stress levels up to 80 kPa. The pores nevertheless become less continuous at 120 kPa net vertical stress. Likely because of a collapse of macropores, which led to the huge drop in the desaturation rate (Fig. 5a) as tortuosity of pore network was increased. Furthermore, as will be discussed later an increase in normal stress level led to breakage of the aggregates due to mechanical loading.

Comparison between stress-dependent SWRCs of GLH and NLG

Figure 4b shows the plots of SDSWRC in terms of degree of saturation against suction on the vertical and horizontal axis respectively for NLG. For this test, the net vertical stress range from zero to 200 kPa. Similarly, to GLH, the specimen at zero stress retains the highest saturation over the suction range considered except in the early portion of the curve. Moreover, a monotonic decrease in water retention capacity for both drying-wetting process was observed for the NLG, even upto 200 kPa. Correspondingly, desaturation rate increases with elevated

stress level for the NLG (Fig. 5a), which is in contrast with what was observed for the GLH and what is commonly reported in the literature (e.g. Salager *et al*., 2013; Ng *et al*., 2016).

The observed water retention behaviour of the NLG on one hand, could be that macropores that are less connected existed in NLG at zero stress condition and hence, led to a lower rate of desaturation (Fig. 5b). On the other hand, increasing stress majorly effects the macropores and that caused a decrease in the average pore size at the macro scale (Koliji et al., 2010). Consequently, an initial bimodal pore size distribution that may have existed in NLG (Akinniyi, 2019) tends to become more uniform and connected (Koliji et al., 2010). The increase in pore uniformity thus causes an increase in the rate of desaturation (Fig. 5b) and hence a decrease in SWRC with an increase in stress level. It worth noting that the magnitude of the rate of desaturation and adsorption is governed by the size and connectivity of macropores (Ng & Menzies, 2014).

Comparing Fig. 4a and b reveals that the SDSWRC for the GLH decreases when there is an increase in net vertical stress up to 80 kPa and then it begins to increase with an increase in net vertical stress. On the contrary, the water retention of the NLG was observed to be decreasing consistently with an increase in net vertical stress even up to the highest stress level considered. The results show quantitatively, that GLH retained more water than NLG within the stress range considered. Furthermore, between the lowest and the highest stress range considered, degree of saturation increased by 4.5 % for GLH, while a decrease of 32.6 % was measured for NLG. Generally, a decrease in suction is associated with an upward movement of the SWRCs (i.e., water uptake by specimen), which is consistent with what is observed for both soils under all loading conditions. The observed upward shift in the wetting path SWRC with a decrease in suction is explained with more emphasis on the rate of adsorption associated with each soil sample. Fig. 5b shows that the adsorption rate decreases with elevated net vertical stress for both GLH and NLG.

Effects of stress on air-entry value (AEV)

In determining SWRC, the specific suction point where a distinct change in the degree of saturation occurs along the drying curve with rise in suction is known as the AEV. At this suction value air begins to enter the soil sample and defines the transition from saturated to unsaturated state. Air Entry Value (AEV) estimated from the curves (Fig. 4) are summarized in Table 4. Fig. 6 presents the evolution of AEV with net vertical stress level for both soils. The results show that the AEVs consistently decrease with an increase in net vertical stress for the GLH. For the NLG, the AEV decreases between 0kPa and 40kPa, thereafter, it shows increasing magnitude with stress level. However, the rate of increment of AEV reduces significantly after 80kPa net vertical stress. The difference between the AEV at 40kPa and 80kPa is about 150% compared to the 4% increase between 80kPa and 200kPa. A similar trend of AEV with net vertical stress was also observed by Oh & Lu (2014) on silty sand decomposed granite. In the literature is it commonly reported that AEV increases when net vertical stress is elevated (Ng & Pang, 2000; Salager *et al*., 2013; Ng *et al*., 2016). A possible explanation for the continuous decrease in AEV for the GLH, and at 40 kPa net vertical stress for the NLG, on one hand, could be due development of fissures in aggregates under relatively lower stress. On the other hand, when the stress level is elevated high enough, the fissures may or may not close depending on the level of stress and suction for a given soil. For the NLG, the increase in AEV as net vertical stress increases suggest closure of the fissures due to stress levels. Sivakumar et al., (2010a) observed that for one-dimensionally compressed samples, the aggregates were fissured at low values of confining stresses. In other words, the one-dimensional static compression caused the aggregates to undergo shear deformation, thus making them susceptible to degradation at a higher degree of saturation. The degradation of the aggregates causes macropores of more uniform size to result, and hence the rate of desaturation increases (see Fig. 5). It should be noted that the sizes of the resulting uniform pores would vary with

stress levels (or level of compression) (Koliji et al., 2010). In the case of the GLH, the continuous decrease in the AEV is because the aggregates are much weaker and hence the number of fissures due to the shear deformation increase with stress levels. Furthermore, the aggregates became more brittle due to drying and degraded under the applied stress, hence led to a 'finer material' to result, and consequently increased the water retention. This implies that the level of aggregates degradation depends on stability of aggregates and stress levels and occurred at a suction value higher than the AEV. Further analysis showed that evolution of aggregate size distribution with stress levels occurred for the GLH. Detailed discussion is provided later (see Fig. 8a).

Volumetric response of GLH and NLG to drying-wetting process.

Figure 7 illustrates the measured changes in void ratio (e) versus suction for the two soils studied. From this figure, the influence of volume change due to stress effects and suction increase can be analysed separately. In Fig. 7a and b, a downward movement of the void ratio curves with stress levels can be observed for both soils. Indicating significant changes in initial void ratios due to compression and thus great modifications in the compaction-induced structure. From this state, suction was increased or decreased to obtain the SDSWRCs with volume change measurements. Fig. 7a shows that the void ratio before drying-wetting ($\boldsymbol{e}_c$) process seems to be independent of suction level in the early and later stages of the drying and wetting process, respectively. At higher suction however, significant changes in the $\boldsymbol{e}_c$ for the samples can be observed in the later stages of drying at varying levels of suction for both soils. On the wetting path, a decrease in suction resulted in swelling of the soil samples at stresses higher than zero. The data shows that the swelling is only noticeable when suction was reduced from 400 to about 50 kPa and remains almost constant throughout the rest of the wetting process for all three samples (i.e., GLH-40, 80 & 120). In the case of the zero net vertical stress sample, it appears void ratio is independent of suction level during the wetting process.

For those samples under higher stresses, it is interesting to observe the changes in void ratio along wetting for given net vertical stress coincides with that of the drying curve of a sample under higher net vertical stress (Fig.7a). In other words, the void ratio curve during wetting for GLH-40 coincides with that of the GLH-80 along the drying path. Accordingly, the GLH-80 coincides with that of the GLH-120 along the drying path. The observed volume change behaviour is consistent with the framework for low activity clays proposed by Gens & Alonso (1992) which was later discussed by Wheeler *et al.* (2003). Based on the framework it can be inferred from results, that for the GLH the influence of suction increase on yield stress in the loading collapse (LC) plane is equivalent to an increase in net vertical stress but may differ in magnitude. This implies drying samples of GLH due to suction increase or increasing the net vertical stress will cause a shift in the yield surface in the LC plane.

Fig. 7b depicts the measured changes in void ratio against suction for the NLG for all five-stress conditions considered. Likewise, to the GLH, the figure shows that the $\boldsymbol{e}_c$ for the NLG appears to be insensitive to both stress state and suction increase in the early stages of drying, with only observable variation associated with the soil sample at 80 kPa net vertical stress.

A compression test on compacted samples showed that the preconsolidation pressure (P_c) for the NLG is around 80 kPa (Ng et al., 2019). The P_c value thus correspond to the net vertical stress value at which the SWRC for NLG-80 was measured, while the 120 and 200 kPa samples were under stresses higher than the P_c. This implies the sample at 80 kPa was within the elasto-plastic region whereas the samples at 120 and 200 kPa were within the plastic region, hence an increase in suction caused plastic volumetric strain in the sample at 80 kPa. On the other hand, to cause similar plastic volumetric responses in a sample at 120 and 200 kPa stress levels, suction values higher than the range considered in this study is required. Contrary to the observation in Fig. 7a, the relative positions of the void ratio curves implies that the influence

of an increase in suction on LC yield stress will vary from that of the NLG (Fig. 7b). The plastic volumetric strain experienced by the sample at 80 kPa therefore resulted in difficulty for water to be absorbed into the specimens. Fig. 5b shows the NLG-80 demonstrated lower rate of water absorption and thus highlight the impact of the reduction in void ratio as suction rises, on the resulting SWRC behaviour. In the case of samples under higher stresses (i.e., NLG-120 & NLG-200), the higher compression caused higher change in void ratio. Therefore, though higher capillarity could develop in those samples, the available pore volume relative to the total volume of soil sample was lower. Consequently, led to a lower total volume of water to be absorbed into NLG-120 & 200 than that of NLG-80. A conclusion can thus be arrived that desaturation and absorption phenomenon of GLH and NLG soils under these stress conditions is governed by the compaction-induced and stress state. It should nevertheless be noted that the compaction-induced state is governed by the stability and how aggregates respond to mechanical loading.

Influence of stress level on the aggregate size distribution

Figure 8 shows the aggregate size distribution of all samples tested for both soils after the SDSWRCs measurements. These curves were obtained by soaking the entire specimen of each test in deionized water for 24 hrs after oven drying at 105 ^{0}C for moisture content determination. The sieve analysis was conducted following the method described in (ASTM, 2004). It should be noted that no mechanical effort was applied to any of the specimens to avoid any influences of external forces on the size of the aggregate. Likewise, no chemical dispersant was added to the deionized water. All the sieve tests were subjected to equal duration (20 min) of shaking in the mechanical shaker.

Fig. 8a depicts the results for the GLH. From the figure a consistent upward shift, in the aggregate size distribution with an increase in net vertical stress is seen. Using the sample under zero net vertical stress as a reference, the continuous upward shift of the curve suggests

subjecting the soil samples to higher stress led to an evolution of aggregate size distribution for the GLH. In simple terms, the larger size aggregates breakdown into smaller sizes as the applied stress was increased. The presence of the smaller size aggregates (or 'finer soil') also caused the soil to begin to hold more water (Fig. 4a). It is thus intuitive for one to expect a corresponding increase in AEV with stress level. The results however show a contrary behaviour (Fig. 6). Moreover, when one focuses on the trend of AEV, it unexpectedly appears to have an inverse relationship with rate of desaturation and the increase in the degree of saturation with suction observed at 120 kPa net vertical stress for the GLH (Fig. 4a). This observation contradicts what is commonly reported in the literature (e.g., Ng & Pang, 2000). Therefore, the increase in the degree of saturation as demonstrated by GLH-120 can only be attributed to the manner in which water is held within aggregate pores under varying suction and stress (Toll, 2000).

The aggregate size distribution for the samples of NLG is presented in Fig. 8b. It is also interesting to observe that the aggregate size distribution curves obtained for all stress conditions considered are similar, which is contrary to what is observed for the GLH. In other words, the aggregate size distribution obtained of the NLG after testing is independent of the stress level considered. This observation implies that the size of the effective 'aggregates' is much stronger and was maintained even under stresses as high as 200 kPa. The effective aggregate size herein refers to the aggregates retained after soil samples were subjected to 24 hrs of soaking, followed by running tap water until the water coming out of the soil was clean. The differences in the response of aggregates to compression as shown by the two soils studied can partly be assessed using the differences in their compressibility index.

The compressibility index measured for the studied soils from isotropic compression tests on comparable specimens are summarized in Table 3. Clearly, the compressibility index of the GLH (i.e., 0.13) is about twice that of the NLG (i.e., 0.07) suggesting that the GLH is

more compressible than NLG. The difference between the compressibility of GLH and NLG is because of the different minerals presents in the studied soils, which is as results parent rock types from which they were formed. The GLH is formed from decomposed phyllitic rock (a metamorphic rock), while the NLG is from granitic rock (intrusive igneous rock). Compared with metamorphic rocks, the intrusive rocks have larger crystal/grain texture due to slower cooling of magma below the earth surface. The slow cooling encourages the growth of larger crystals causing reduced pore size, thereby affecting compressibility (Loughnan, 1969). Moreover, the crystals in the weathered state are cemented together by the sesquioxides, resulting in the aggregation which affects the particle size distribution as shown in Fig. 1. The conclusion, therefore, is that stress levels and present minerals should be considered in describing the SDSWRC for lateritic soils.

Effects of mineral type on the stability of aggregates

The XRD results showed that apart from the common minerals in both soils, halloysite and goethite were unique to GLH and NLG, respectively (see Table 2). For the halloysite minerals, although many forms exist, the most common morphology found in soils is the elongated tubule (Joussein et al., 2005; Yu et al., 2016). According to Yu et al. (2016), this morphology occurs when the platy morphology of Kaolinite is distorted, and two main forms may occur depending on the moisture content. The two forms were represented by a general molecular formula, as $Al_2Si_2O_5(OH)_4.nH_2O$, where n is equal to 2 and 0 for the hydrated and dehydrated forms respectively. These forms occur when the monomolecular layer of water between the Kaolin sheets of which halloysite is formed is lost (Newill, 1961). The loss of the water leads to the rolling of the Kaolin sheet into the elongated tubule. The dehydration is influenced by several factors such as relative humidity, temperature, and drying history (Joussein et al. 2005; Yu et al. 2016). Newill (1961) and Yu et al. (2016) believe that this dehydration occurs when the moisture content or relative humidity reduces by 10 % and 40 %

respectively. Hence, the environmental conditions under which these soils were formed plays a key role in the type of secondary mineral found in them. This also implies that an increase in suction during drying could also have a diverse influence on the volumetric responses of these soils (e.g., see GLH-0 and NLG-0 in Fig. 5). Under Transmission electron microscopy (TEM), Yu et al. (2016) observed that the elongate tubules have a high aspect ratio (length/diameter) (see the image in Fig. 8a). Hence, it is easier for the aggregates associated with these halloysite minerals to break under higher stresses. Joussein et al. (2005) have observed similar morphology.

Regarding the goethite minerals found in the NLG, they are commonly nanometers (nm) in size and needle-like in shape and usually aggregates into sizes of 10s to 100s of microns (Ding & Pacek, 2008) (see the image (i) and (ii) in Fig. 8b). Otalvaro et al. (2016) observed that weathered soils that contain a substantial amount of goethite mineral had large-structure-supported voids when the particles aggregates. A structure supported void at nano-scale in limonite soil containing a significant proportion of goethite has been reported (Airey et al., 2012). Furthermore, some studies has shown that aggregated goethite can only be de-aggreagted back to the nano level at very low pH (i.e., 3) or utilizing high-energy resource because of their stability in neutral conditions (pH = 7) (Blakey & James, 2003; Ding & Pacek, 2008). Besides, halloysite has a hardness of 1-2 while goethite has 5.5 on the Mohs scale (Mukherjee, 2012). The difference in hardness likely affects stiffness of the aggregates and the soil skeleton and consequently affects compressibility. These differences in physical and chemical properties thus influence the stability of the aggregates in the soils under stresses.

Based on these physical properties of the minerals, the observed volume change behaviour in Fig. 7 implies there are two main mechanisms controlling the volume change response of the soils studied. First, the aggregates in both soils experienced rearrangement upon loading, which accounts for the downward movement of the *e* versus suction curves (Fig. 7a

and b). The reorganization of the aggregates led to pores of a uniform size to result and consequently increases the rate of desaturation for the NLG (see Table 4). The dependency of pore size distribution in a soil sample on the applied stress has been demonstrated experimentally (Burton et al., 2014) and numerically (Zhou & Ng, 2014). The rearrangement of the aggregates could also cause fissures which may or not close during drying, for a given stress condition and suction levels. The second mechanism is the evolution of aggregate sizes with stress level, which is evident in the aggregates size distribution analysis for different stress conditions as presented in Fig. 8a. The parent rock from which the soils are form and thus the resulting minerals, govern the aggregates response to stress levels. The simple conclusion is that the SDSWRCs of lateritic clays studied is controlled by the compaction-induced state, stress and suction levels. The implication, therefore, is that the SDSWRCs of lateritic soils that can form aggregation cannot be described using only the particle size distribution or void ratio.

Influence of vertical stress on the size of hysteresis loop

In Fig. 4, there is a marked hysteresis between the drying and wetting curves for all specimens for both soils. Thus, the wetting curves does not returns to the initial positions before initiating drying (Fig. 4a and b). It is important to understand how the size of the hysteresis loop response to stress increase because the size of the loop is equivalent to the lost in the component of shear strength contributed by water meniscus. The relative position of the drying and the wetting curves defined the hysteresis loop. Using the approach proposed by Lu & Khorshidi, 2015 to analyses the degree of hysteresis does not give a better indication of how the size of the hysteresis loop response to the stress levels. This is because the changes in pore size distribution caused by increase in stress affects the degree of hysteresis (Li et al., 2011; Zhou & Ng, 2014) and also the size of the hysteresis loop. Considering the area enclosed by the drying and wetting curves, the size of the hystresis loop was estimated using the 8.5 version

of the "*OriginPro software*", which approximate the area as a polygon. The result is summarized in Fig. 9.

The calculated size of the loop for the studied soils are ploted against stress at which the samples were tested in Fig.9. The results for GLH is presented as open circles connected with broken lines. The results show that the loop size increases as stress level was elevated, however, at a decreasing rate. The loop size reaches a optimum value at net vertical stress of 80 kPa and then begins to drop as the stress increases to 120 kPa. The trend of the size of the loop with stress levels follows, is thus consistent with what was reported for a fine grain soil (completely decomposed volcanic (CDV)) by (Ng & Pang, 2000b). It however has an inverse relationship with the trend of the measured soil water retention curves (Fig. 4a). The decrease in the size of the loop is marked when the sizes of aggregates are significantly reduced at 120 kPa net vertical stress (see Fig. 8a) for the GLH.

Likewise, for the NLG, the size of the loop experienced a sharp rise as net vertical stress reaches 40 kPa. The sharp rise droped gradual afterwards when net vertical stress was elevated to 80 kPa. The decrease is observed to be followed by a sharp increase at higher stress. Quantitatively, the size of the loop rose by about 47% with net vertical stress up to 80 kPa, and then fell by about 18% as the stress was raised to 120 kPa for the GLH. Regarding the NLG, the size of the loop increases by over 200% when net vertical stress increases from zero to 200 kPa. The trend of the hysteresis loop size with stress levels suggests that below 40 kPa stress, hysteresis is majorly controlled by the rearrangement of the aggregated particles in both soils. Above 40 kPa, however, different degree of fissuring and (or) breakage of the aggregates is likely initiated. Hence, the differences in the loop size as the stress exceeds 40 kPa. Moreover, shrinkage collapse occurred during the drying process (Fig. 7b), leading to about 7% of volume change for the NLG. The high-volume change subsequently added to the difficulty for water

to be drawn out or absorbed into the samples and thus resulted a large difference between the water content for the drying and wetting process. This suggests that suction effects on the loop size is dependent on the stress levels. Thus, a soil sample subjected to a higher stress becomes denser and consequently reduces effects of suction on its volume change and PSD for the NLG.

The conclusion is that the behaviour of the hysteresis loop is directly affected by compaction-induced and stress state prior to drying and wetting and is governed by aggregates stability. Furthermore, the inverse relationship between hysteresis loop and net vertical stress reported elsewhere (Ng & Menzies, 2014) can not be generalized for all soils.

Microstructure Investigation

The structure of soil and the corresponding pore size distribution (PSD) is derived from the arrangement of the particles which affects the overall mechanical and hydro-mechanical properties (Thom *et al*., 2007; Burton *et al*., 2014). One of the common ways of qualitatively studying soil structure is through visual inspection of images.

The SEM images at different magnifications of soils studied are presented in Fig. 9. Fig. 9a and b, show images taken at a magnification of 1000 times for the GLH and NLG, respectively. Many free clay particles can be observed in the GLH (Fig. 9a), while almost no free clay particles can be observed in the NLG (Fig. 9b), though both soils contain 42% clay content. Moreover, smaller-size pores are also visible in the GLH, while only a fissure (crack) can be seen in NLG with no other visible pores. This can be attributed to the fact that the fine contents have form aggregation due to the significant content of sesquioxides in both soils. The aggregates in GLH however, break down into smaller size aggregate than those in NLG under compression due to the lower strength provided by halloysite than goethite mineral to the aggregates in GLH and NLG, respectively.

Comparing the images at a magnification of 2000 times in Fig. 9c and d, free clay particles are still visible in the GLH sample and aggregates size are relatively smaller. In the case of the NLG, relatively larger-size aggregates can be observed and almost no isolated clay particles are seen. On magnifying to 4000 times, relatively smaller size aggregates can be found in GLH (Fig. 9e) than in NLG (Fig. 9f). Moreover, large-size macropores/fissure are visible and appear to be connected in the NLG whereas almost no visible pores exist in the GLH. The higher degree of aggregation observed in both soils is mainly caused by the sesquioxides (Fe_2O_3 + Al_2O_3) contents found in the soils (see Table 2). These aggregates however, differ in strength under normal stress, mainly because of the differences in stability provided by minerals in the soils. This SEM images is thus consistent with the result in Fig. 8, nevertheless, contradicts the degree of petrifaction (Dp) (Table 1) measured for the soils. The parameter Dp is a measure of the aggregation potential and level of stability of the aggregates to be expected in given soil (Nascimento, 1964). This thus emphasizes the influence of mineral type on the stability of aggregates. Therefore, the existence of larger-size aggregates in NLG is mainly because of the additional stability provided by the goethite (FeO(OH)) mineral found in the soil. Besides, the presence of this mineral basically increases the iron (Fe^{2+}) (see Table 2) in the soil, which is well known to have cementation effects (e.g. Sunil & Krishnappa, 2012).

It is important to be pointed out that, the water retention samples of both soils were compacted on the dry of OMC, hence the specimens were associated with bimodal PSD at the initial state. MIP test on a sample from the same soil by Akinniyi, 2019 shows that the NLG in the compacted state is associated with bimodal PSD. Bimodal PSD in compacted samples is commonly reported (Burton *et al.*, 2014; Vanapalli *et al.*, 1999). Therefore, those sample under zero net vertical stress condition maintained the bimodal pore size distributions which were less connected. As a result, they were associated with a lower rate of desaturation and consequently retained more water (Fig. 4a and b). Fig. 5a indicates that the highest rate of

desaturation corresponds to 80 kPa net vertical stress for the GLH and decreases at 120 kPa net vertical stress, with a corresponding improvement in the water retention ability. The improvement in the SDSWRC for the GLH (Fig. 4a) thus implies that as stress levels increases, and the aggregates become smaller, uniform pore-size are maintained in samples under lower stress as suction is increased. The size of the uniform pore however, is reduced at higher stress thus caused a reduction in the rate of desaturation (Fig. 5a) (Ng and Pang, 2000a) and hence an increase in the water retention curve. For NLG, the highest rate of desaturation is associated with the samples that were subjected to the highest stress. On one hand, it is possible that at higher stresses, aggregates continuously moved to occupy those larger macro void (Sivakumar et al., 2006) found in the NLG from the SEM. Hence, macropores that are of uniform in size and highly connected, continuously evolved and consequently increased the rate of desaturation (Fig. 5a) and water retention capacity reduced (Fig. 4b). On the other hand, cracks are seen in the SEM images for the NLG and thus could have contributed to the higher rate of desaturation.

Effects of aggregation on pore size distribution (PSD) at nanoscale and specific surface area (SSA)

It has been reported that lateritic soils that contain the mineral goethite usually have many structure-supported voids even at nanoscale (Airey et al., 2012; Otalvaro et al., 2016a). Therefore, the possible existence of structure-supported voids in the NLG and GLH at the nano level was also investigated. This is to show whether the presence of nano pores is a function of mineralogy or an intrinsic property of lateritic clays. It is likely not possible for the structure-supported void at the nanoscale to be identified at the level of magnification studied with the SEM technique. Therefore, it was verified by measuring quantitatively the total pore voids (or volume) (TPV) per unit mass of a dry sample and pore size distribution at nano scale for both soils, using the BET method.

The data show that both soils contain similar total pore volume (Table 1). It is interesting however to note the rate of change in pore volume during BET test. The rate of change of pore volume for both GLH (open circles) and NLG (open triangles) is presented in Fig. 11. Although similar TPV was measured for both soils, the GLH has pore size around 20 nm been the most dominate pores, while pore sizes of about 3.5 nm and 18 nm are dominant in the case of the NLG. This result implies that different PSD exist in the soils studied even at nanoscale. However, for a given dry mass, TPV at the nanoscale may not vary significantly regardless of the type of mineral present. The simple conclusion is that although nano pores is an intrinsic property of lateritic (or chemically weathered) soils, mineralogy influences the PSD. Nevertheless, TPV per unit mass at the nano-scale is independent of mineralogy for lateritic soils studied.

Another interesting result is the SSA measured from the same BET test (Table 1). The results show that besides the differences in the PSD at the nano-scale, the SSA of the existing minerals also varies significantly. The data shows that the SSA of NLG is over 50% higher than that of GLH. This implies that NLG may hold more water than GLH if both soils are prepared at the same state and dry beyond the residual suction, which is defined as 1500 kPa by Vanapalli et al. 1999. This is because Khorshidi et al. 2002 showed there exist a direct link between SWRC and SSA at suction levels beyong residual suction.

Conclusions

The SDSWRCs of two lateritic clays with two different predominant minerals have been studied, discussed, and compared. The two soils have halloysite (i.e., GLH) and goethite (i.e., NLG) as their predominant mineral. From the experimental results the conclusions drawn include the following:

1. A significant change in the particle size distribution between dry and wet sieve tests was observed for the studied soils. Furthermore, an evolution of aggregate size distributions with stress level was observed for the GLH, while that of NLG was independent of stress level. The two soils contain a similar amount of sesquioxide contents (i.e., GLH = 36% & NLG = 38%), which enhances aggregation. The aggregate responded differently to stress because of the differences in strength provided to the aggregates by the halloysite and goethite in GLH and NLG, respectively. Besides, the differences in the hardness of the halloysite and goethite imply different binding strengths to the aggregates in GLH and NLG, respectively.

2. The GLH generally retained higher water content than the NLG for any given suction, though GLH had a higher initial void ratio. Nevertheless, both types of specimens exhibit lower water retention capacity at higher stress except at 120 kPa net vertical stress for GLH. This is mainly because the presence of sesquioxides enhances aggregation in both soils. However, aggregate sizes of about 20 to 30 μm and 10 to 11 μm at the same magnification were observed in the NLG and the GLH respectively, as revealed by the SEM images. As a result, larger-size macropores exist in the NLG than the GLH and hence the former has lower water retention capacity than the latter. Moreover, the aggregates in the GLH broke down with an increase in stress, whereas those in NLG virtually remained the same as revealed by the aggregate size distribution after testing.

3. It is found that AEV decreases consistently with an increase in net vertical stress for the GLH, though an increase SDSWRC was observed at 120 kPa. In the case of the NLG, generally, AEV increased as net vertical stress was elevated, except at 40 kPa. The continuous decrease in AEV for the GLH, and the drop at 40 kPa for the NLG could possibly be fissures that occur in aggregates under relatively lower stress. When the stress level is elevated, however, based on the soil type, the fissures may or may not close. For the NLG, the closure

of the fissures with elevated stress led to an increase in AEV. Moreover, an increase in suction caused the aggregates to become more brittle and breakdown into a smaller size under stress for the GLH. This implies that the SDSWRC of lateritic soils is controlled by the compaction-induced state and resulting soil structure associated with stress and suction levels.

4. It was observed that both soils demonstrate an increase in the rate of desaturation with an increase in stress, however, some differences arose. GLH and NLG exhibit a lower rate of desaturation at 120 and 80 kPa net vertical stresses, respectively. Hence, the rates of desaturation were observed to decrease at net vertical stress of 120 kPa and thus caused a significant decrease in the rate of desaturation and led to an increase in water retention capacity for GLH. For the NLG, at 80 kPa sample experienced shrinkage collapse during the drying process. The rate of adsorption was observed to increase with a decrease in stress for both soils. The observed water retention behaviour is mainly because the aggregates experience rearrangements in both soils and subsequently breakdown into a smaller size for the GLH. In contrast, the rearrangement of aggregates in NLG is possibly associated with only fissuring rather than breaking down completely as shown by the microscopic image analysis and led to more water to be removed easily from the soil when suction was increased.

5. For the GLH the size of the hysteresis loop increases by 47% with net vertical stress up to 80 kPa, the value then decreases by 18% as the stress was increased to 120 kPa. Regarding the NLG, the size of the hysteresis loop increases by over 200% with net vertical stress increases from zero to 200 kPa. Shrinkage-collapse with suction increase occurred in NLG at 80 kPa and lead to a shrink in size of the loop. The manner in which the hysteresis loop responded to net vertical stress is mainly because of the different response of the aggregates to stress state in the two soils. Therefore, an inverse relationship between the hysteresis loop and net vertical stress cannot be generalized but rather be considered soil dependent.

Acknowledgements

The authors would like to acknowledge the financial support from the research grants 16207621, 15205721 and AoE/E-603/18 from the Research Grants Council of HKSAR.

Acronym	**Meaning**
AEV	Air-entry value
BET	Brunauer-Emmett-Teller
e	Void ratio
e_c	Void ratio before drying and wetting
CH	Sandy fat clay
CL	Sandy lean clay
D_h	Degree of hysteresis
GLH	Ghana lateritic soil containing Halloysite mineral
LC	Loading collapse
OMC	Optimum moisture content
NLG	Nigeria lateritic soil containing Goethite mineral
PPA	Pressure plate apparatus
P_c	Preconsolidation pressure
PSD	Pore size distribution
SEM	Scanning electron microscopy
SSA	Specific surface area
S_r	Degree of saturation
SWRC	Soil water retention curve

SDSWRC	Stress-dependent soil water retention curve
TPV	Total pore volume
XRF	X-ray fluorescence
XRD	X-ray diffraction

References

Airey, D., Suchowerska, A., & Williams, D. (2012). Limonite – a weathered residual soil heterogeneous at all scales. *Géotechnique Letters*, 2(3), 119–122.

Akinniyi, D. B. (2019). *Compressibility and shear behaviour of saturated and unsaturated lateritic clay rich in sesquioxide*. The Hong Kong University of Science and Technology, Clear Water Bay, Kowloon, Hong Kong.

Ampadu, P. S. I. K., & Nocilla, P. A. (2017). Characterizing Lateritic Soils Strength and Compressibility of Lateritic Soils, (August), 1–54.

ASTM. (2004). *Standard test methods for particle-size distribution (gradation) of soils using sieve analysis*. ASTM International.

Aubertin, M., Mbonimpa, M., Bussière, B., & Chapuis, R. P. (2003). A model to predict the water retention curve from basic geotechnical properties. *Canadian Geotechnical Journal*, 40(6), 1104–1122.

Burton, G. J., Sheng, D., & Campbell, C. (2014). Bimodal pore size distribution of a high-plasticity compacted clay. *Géotechnique Letters*, 4(2), 88–93.

Delage, Pierre, Tessier, D., & Marcel-Audiguier, M. (1982). Use of the Cryoscan apparatus for observation of freeze-fractured planes of a sensitive Quebec clay in scanning electron microscopy. *Canadian Geotechnical Journal*, 19(1), 111–114.

Ding, P., & Pacek, A. W. (2008). De-agglomeration of goethite nano-particles using ultrasonic comminution device. *Powder Technology*, 187(1), 1–10.

FAO, 1989. Soil Map of the World. ISRIC, Wageningem, pp. 138 (FAO.UNESCO Technical Paper, 20).

Gens, A., & Alonso, E. E. (1992). A framework for the behaviour of unsaturated expansive clays. *Canadian Geotechnical Journal*, 29(6), 1013–1032.

Joussein, E., Petit, S., Churchman, J., Theng, B., Righi, D., & Delvaux, B. (2005). Halloysite clay minerals – a review. *Clay Minerals*, 40(4), 383–426.

Khorshidi, M., Asce, S. M., Lu, N., Asce, F., Akin, I. D., Asce, S. M., … Asce, M. (2002). Intrinsic Relationship between Specific Surface Area and Soil Water Retention, 143(1), 1–10.

Koliji, A., Vulliet, L., & Laloui, L. (2010). Structural characterization of unsaturated aggregated soil. *Canadian Geotechnical Journal*, 47(3), 297–311.

Li, J. H., Zhang, L. M., & Li, X. (2011). Soil-water characteristic curve and permeability function for unsaturated cracked soil. *Canadian Geotechnical Journal*, 48(7), 1010–1031.

Loughnan, F. C. (1969). Chemical weathering of the silicate minerals, (549).

Lu, N., & Khorshidi, M. (2015). Mechanisms for Soil-Water Retention and Hysteresis at High Suction Range. *Journal of Geotechnical and Geoenvironmental Engineering*, 141(8), 04015032.

Miguel, M. G., & Vilar, O. M. (2009). Study of the water retention properties of a tropical soil. *Canadian Geotechnical Journal*, 46(9), 1084–1092.

Mukherjee, S. (2012). *Applied mineralogy: applications in industry and environment*. Springer Science & Business Media.

Murray D. Fredlund, D.G. Fredlund, G.W. Wilson. (1994). Prediction of the SWCC from grain size distribution and volume mass properties.

Nascimento, U. (1964). Swelling and petrifaction of lateritic soils.

Newill, D. (1961). A Laboratory Investigation of Two Red Clays from Kenya. *Géotechnique*, 11(4), 302–318.

Ng, C. W. W., & Menzies, B. (2014). *Advanced unsaturated soil mechanics and engineering.* CRC Press of Taylor & Francis Group, London and NY. ISBN: 978-0-415-43679-3.

Ng, C. W., & Pang, Y. W. (2000a). Experimental investigations of the soil-water characteristics of a volcanic soil. *Canadian Geotechnical Journal*, 37(6), 1252–1264.

Ng, C.W.W. & Pang, Y.W. (2000b). Influence of stress state on soil-water characteristics and slope stability. Journal of Geotechnical and Geoenvironmental Engineering 126, No. 2. 157-166.

Ng, C.W.W., Akinniyi, D. B., Zhou, C., & Chiu, C. F. (2019). Comparisons of weathered lateritic, granitic and volcanic soils: Compressibility and shear strength. *Engineering Geology*, *249*, 235–240.

Ng, C. W. W., Owusu, S. T., Zhou, C., & Chiu, A. C. F. (2019). Effects of sesquioxide content on stress-dependent water retention behaviour of weathered soils. *Engineering Geology*, *266*(December 2019), 105455.

Ng, C. W. W., Sadeghi, H., Hossen, S. B., Chiu, C. F., Alonso, E. E., & Baghbanrezvan, S. (2016). Water retention and volumetric characteristics of intact and re-compacted loess. *Canadian Geotechnical Journal*, *53*(8), 1258-1269.

Ng, C. W. W., Zhang, Q., Zhou, C., & Ni, J. (2022). Eco-geotechnics for human sustainability. *Science China Technological Sciences*, *65*(12), 2809-2845.

Ng, C.W.W., Zhou, C. & Chiu, C.F. (2020). Constitutive modelling of state-dependent behaviour of unsaturated soils: an overview. Acta Geotechnica 15, 2705-2725.

Oh, S., & Lu, N. (2014). Uniqueness of the suction stress characteristic curve under different confining stress conditions. *Vadose Zone Journal*, *13*(5), 1539-1663.

Otalvaro, I. F., Neto, M. P. C., Delage, P., & Caicedo, B. (2016b). Relationship between soil

structure and water retention properties in a residual compacted soil. *Engineering Geology*, 205, 73–80.

Penumadu, D., & Dean, J. (2000). Compressibility effect in evaluating the pore-size distribution of kaolin clay using mercury intrusion porosimetry. *Canadian Geotechnical Journal*, 37(2), 393–405.

Perera, Y. Y., Zapata, C. E., Houston, W. N., & Houston, S. L. (2005). Prediction of the soil-water characteristic curve based on grain-size-distribution and index properties. In *Advances in Pavement Engineering* (pp. 1–12).

Salager, S., Nuth, M., Ferrari, a., & Laloui, L. (2013). Investigation into water retention behaviour of deformable soils. *Canadian Geotechnical Journal*, 50(2), 200–208.

Sivakumar, V., Sivakumar, R., Murray, E. J., Mackinnon, P., & Boyd, J. (2010). Mechanical behaviour of unsaturated kaolin (with isotropic and anisotropic stress history). Part 1: wetting and compression behaviour. *Géotechnique*, 60(8), 581–594.

Sivakumar, V., Tan, W. C., Murray, E. J., & McKinley, J. D. (2006). Wetting, drying and compression characteristics of compacted clay. *Géotechnique*, 56(1).

Sivakumar, V., & Wheeler, S. J. (2000). influence of compaction procedure on the mechanical behaviour of an unsaturated compacted clay. Part 1: Wetting and isotropic compression. *Géotechnique*, 50(4), 359–368.

Sunil, B. M., & Krishnappa, H. (2012). Effect of Drying on the Index Properties of Lateritic Soils. *Geotechnical and Geological Engineering*, 30(4), 869–879.

Thom, R., Sivakumar, R., Sivakumar, V., Murray, E. J., & Mackinnon, P. (2007). Pore size distribution of unsaturated compacted kaolin: the initial states and final states following saturation. *Géotechnique*, 57(5), 469-474.

Toll, D. G. (2000). The influence of fabric on the shear behaviour of unsaturated compacted soils. In Advances in unsaturated geotechnics. *ASCE*, 222–234.

Vanapalli, S. K., Fredlund, D. G., & Pufahl, D. E. (1999). Influence of soil structure and stress history on the soil–water characteristics of a compacted till. *Géotechnique*, 51(6), 573–576.

Wheeler, S. J., Sharma, R. S., & Buisson, M. S. R. (2003). Coupling of hydraulic hysteresis and stress–strain behaviour in unsaturated soils. *Géotechnique*, 53(1), 41–54.

Yu, L., Wang, H., Zhang, Y., Zhang, B., & Liu, J. (2016). Recent advances in halloysite nanotube derived composites for water treatment. *Environmental Science: Nano*, 3(1), 28–44.

Zhang, F., Cui, Y. J., & Ye, W. M. (2018). Distinguishing macro- and micro-pores for materials with different pore populations. *Géotechnique Letters*, 8(2), 102–110.

Zhang, X. W., Kong, L. W., Cui, X. L., & Yin, S. (2016). Occurrence characteristics of free iron oxides in soil microstructure: evidence from XRD, SEM and EDS. *Bulletin of Engineering Geology and the Environment*, 75(4), 1493–1503.

Zhou, C., & Ng, C. W. W. (2014). A new and simple stress-dependent water retention model for unsaturated soil. *Computers and Geotechnics*, 62, 216–222.

Table 1. Basic properties of the two soils studied.

Index Properties	Soil type	
	GLH	NLG
Standard compaction Test		
Maximum dry density: Mg/m^3	1548	1696
Optimum water content: %	25	20
Grains size distribution		
Sand content: %	36	42
Silt content: %	22	16
Clay content: %	42	42
Specific gravity	2.75	2.67
Atterberg limits	50	44
Liquid limit: %	29	24
Plastic limit: %	21	20
Plasticity index: %		
Soil classification based on USCS (ASTM, 2011)	Sandy fat clay (CH)	Sandy lean clay (CL)
Specific surface area (m^2/g)	23	35
Total nano pore volume (mil/g)	0.13	0.13
Degree of petrifaction (D_p) (%)	470	414

NB: GLH = Ghana laterite with Halloysite; NLG = Nigeria lateritic with Goethite; Dp = ratio of shrinkage limit to absorption limit (Ng et al., 2019).

Table 2. Chemical and mineralogical properties of the two soils studied.

Oxide and Mineral	GLH	NLG
SiO_2	62%	60%
Fe_2O_3	4%	10%
Al_2O_3	32%	28%
Common minerals	Quartz, Hematite, Kaolinite	
Unique Mineral	**Halloysite**	**Goethite**

Table 3. Test Program.

Soil Type	Test ID	Net stress (kPa)	Initial void ratio after compaction (e_i)	Void ratio prior to drying and wetting (e_c)	Compressibility index (λ)
GLH	GLH-0	0	0.720	0.720	0.13
	GLH-40	40		0.689	
	GLH-80	80		0.676	
	GLH-120	120		0.669	
NLG	NLG-0	0	0.670	0.670	0.07
	NLG-40	40		0.647	
	NLG-80	80		0.636	
	NLG-120	120		0.626	
	NLG-200	200		0.601	

Table 4. Parameters estimated from the measured SWRCs.

Soil type	Test ID	Net stress (kPa)	AEV (kPa)	Desorption rate (10^{-4}) (kPa^{-1})	Adsorption rate (10^{-4}) (kPa^{-1})	Hysteresis loop size (kPa)
GLH	GLH-0	0	2.6	596	21	3.8
	GLH-40	40	2.4	629	7	5.5
	GLH-80	80	2.3	864	6	5.6
	GLH-120	120	2.0	503	1	4.6
NLG	NLG-0	0	1.9	370	77	1.9
	NLG-40	40	1.0	390	50	4.6
	NLG-80	80	2.5	470	43	4.3
	NLG-120	120	2.5	640	47	5.1
	NLG-200	200	2.6	707	16	6.1

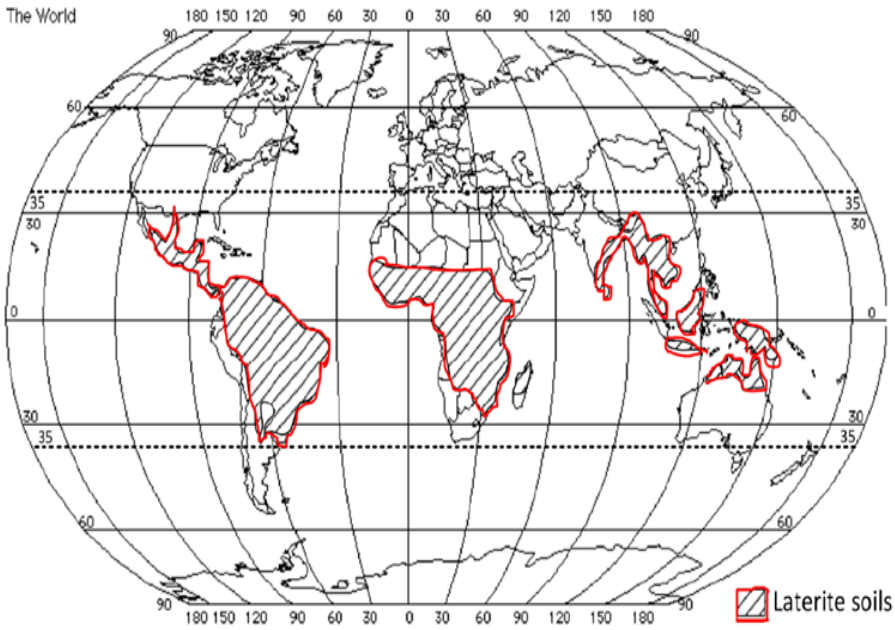

Figure 1. Global distribution of laterites and lateritic soils (after CIRIA, 1995).

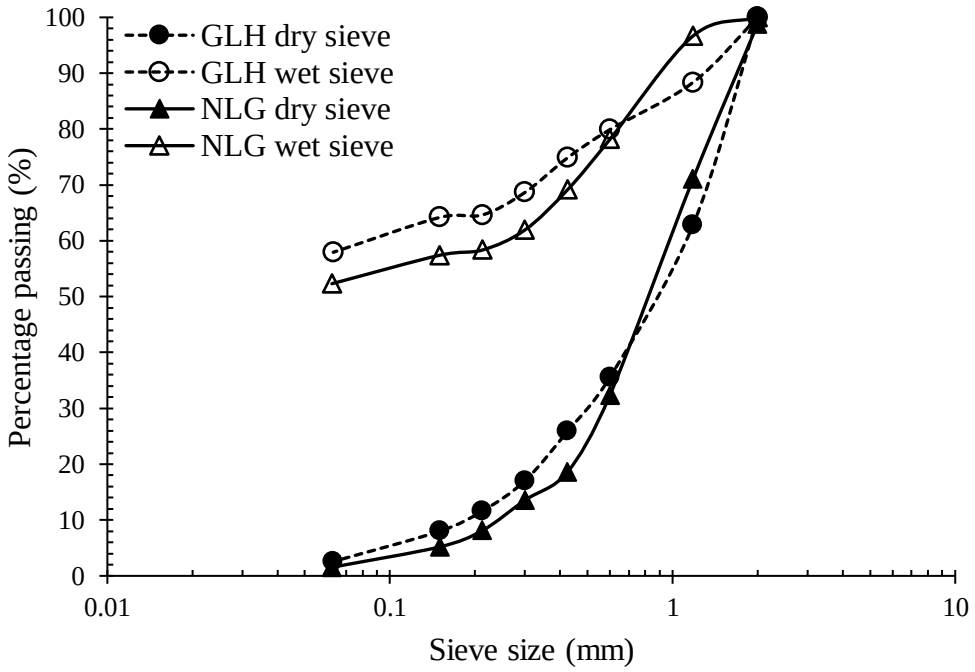

Figure 2. Particle size distributions of the two soils.

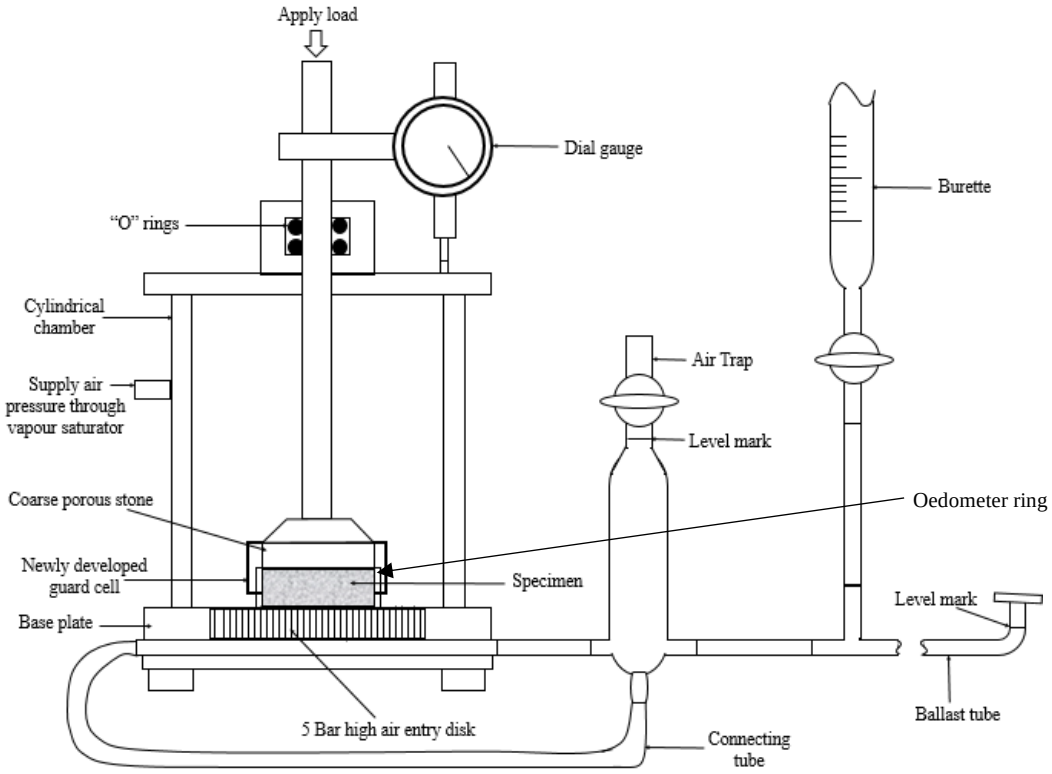

Figure 3. Schematic diagram of improved stress-controllable pressure plate apparatus (by Ng et al., 2019 **after** Ng & Pang, 2000**).**

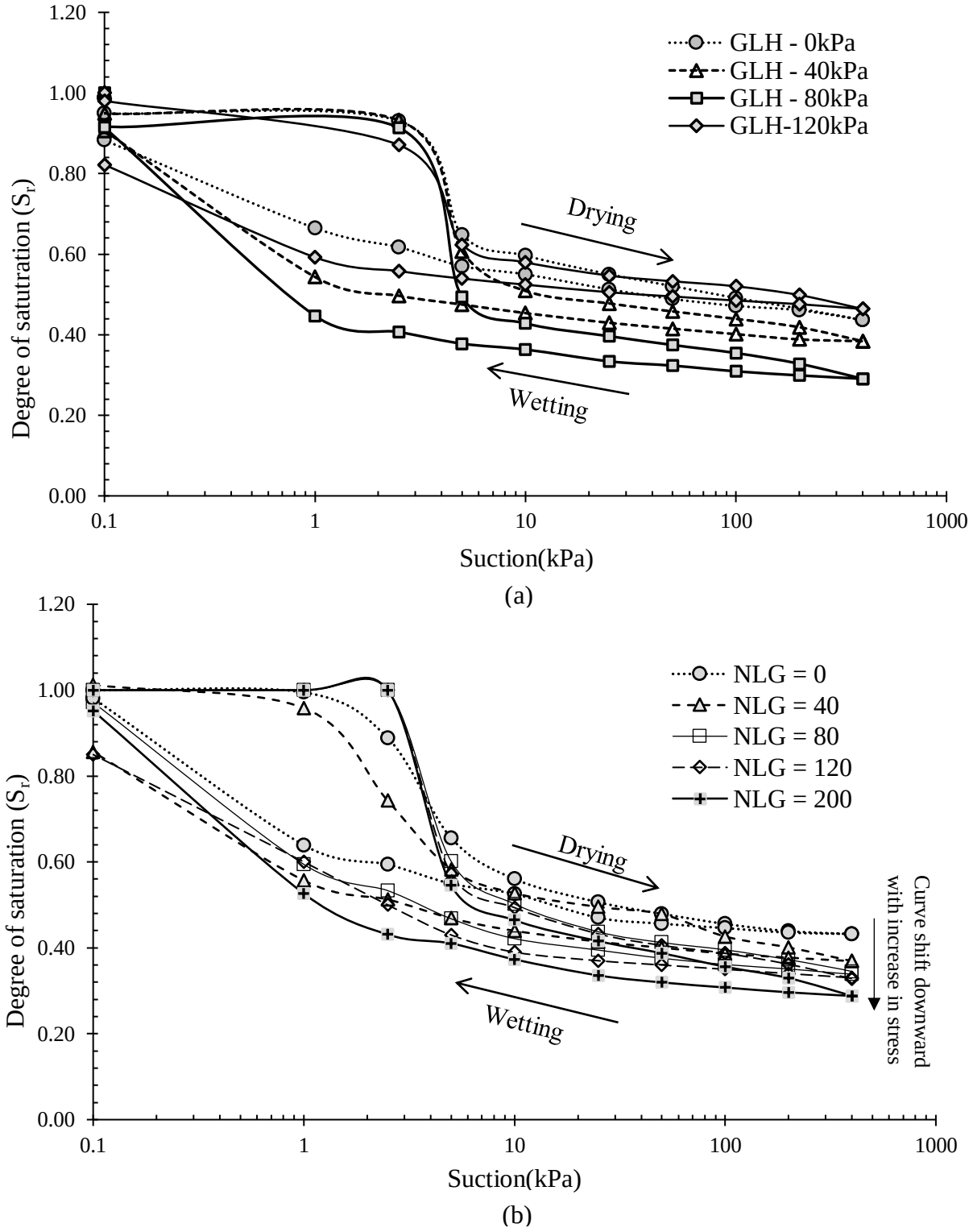

Figure 4. SDSWRC in terms of volumetric water content against suction under different net stresses. (a) for GLH; (b) for NLG.

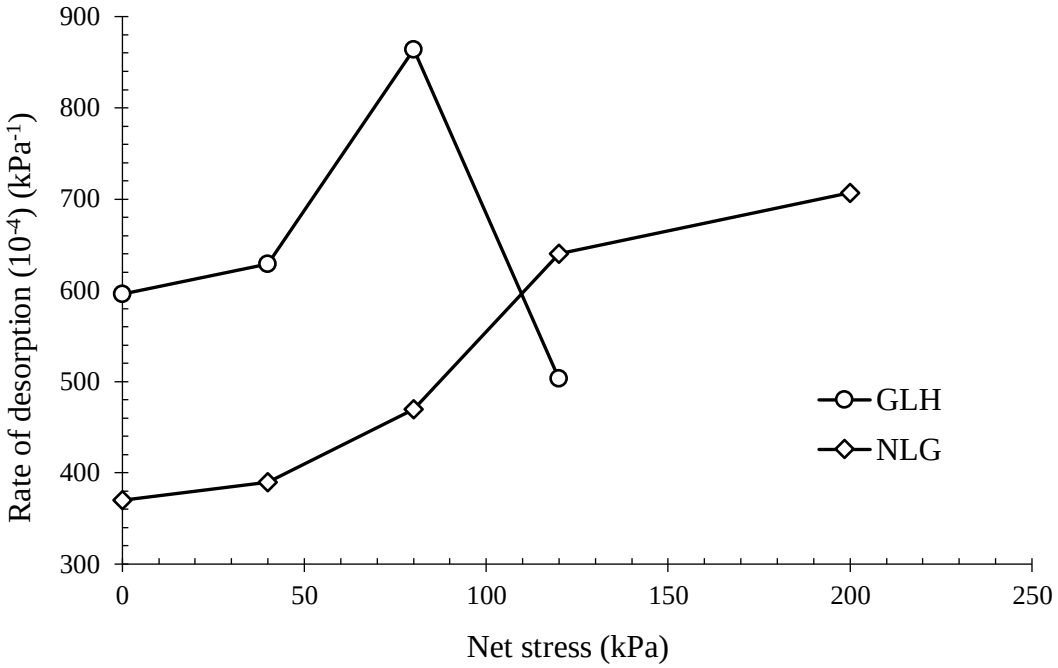

(a)

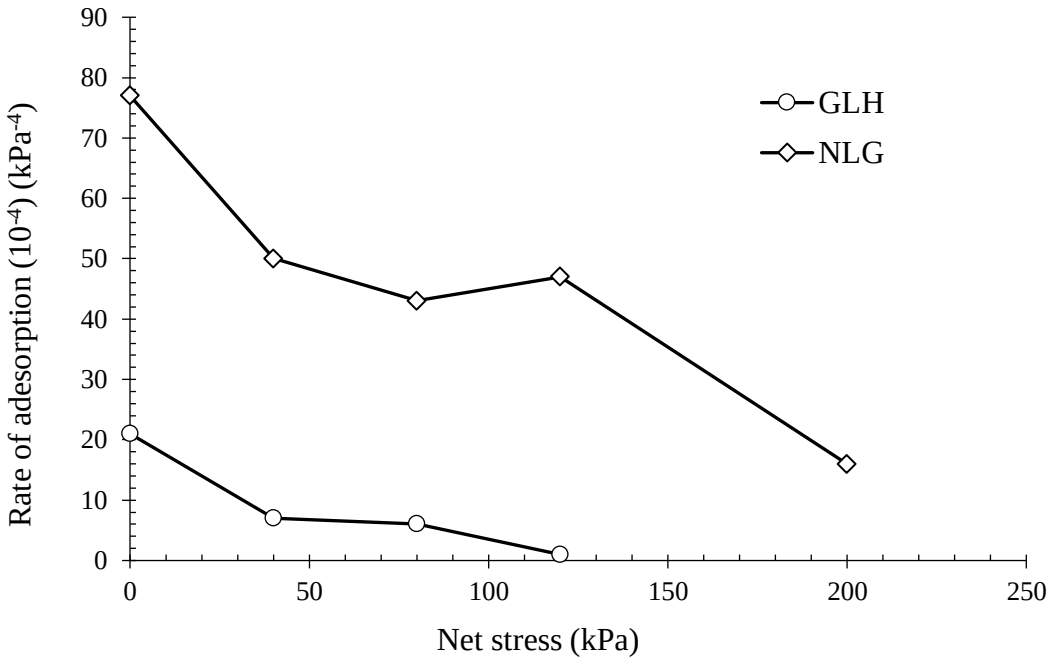

(b)

Figure 5. (a). Rate of desorption; (b). Rate of Adsorption for studied soils.

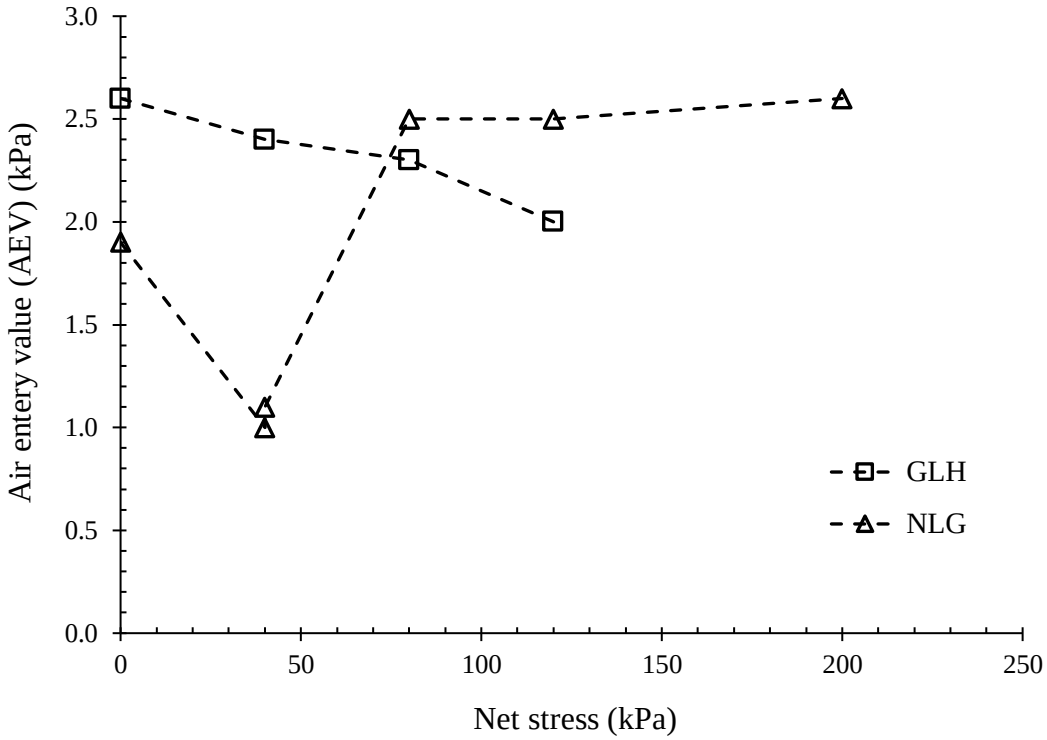

Figure 6. Influence of net stress on air entry value (AEV).

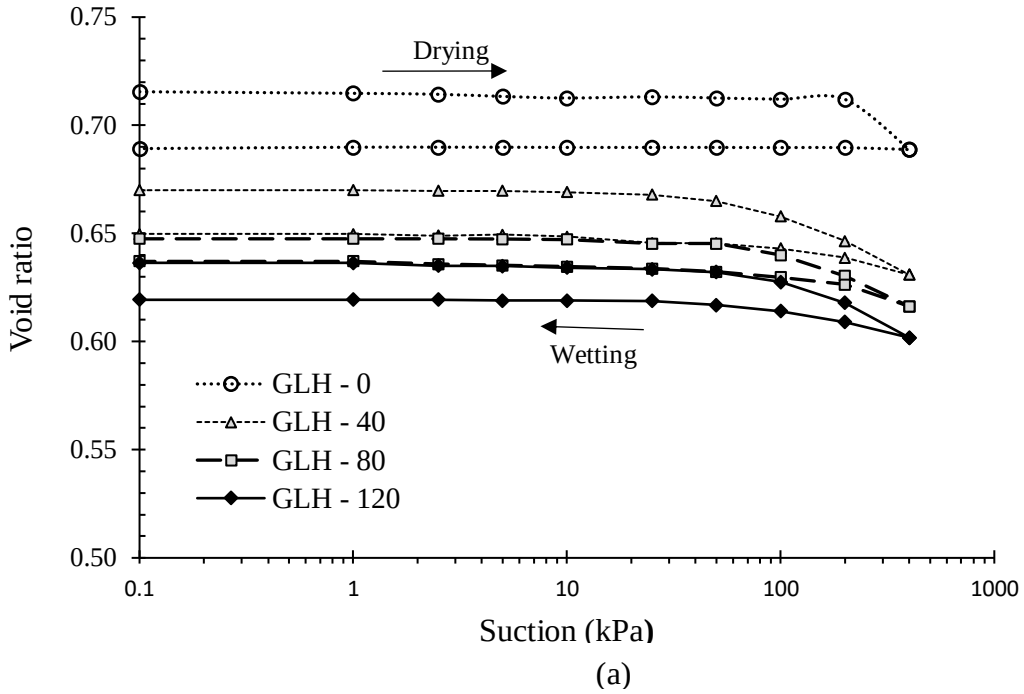

(a)

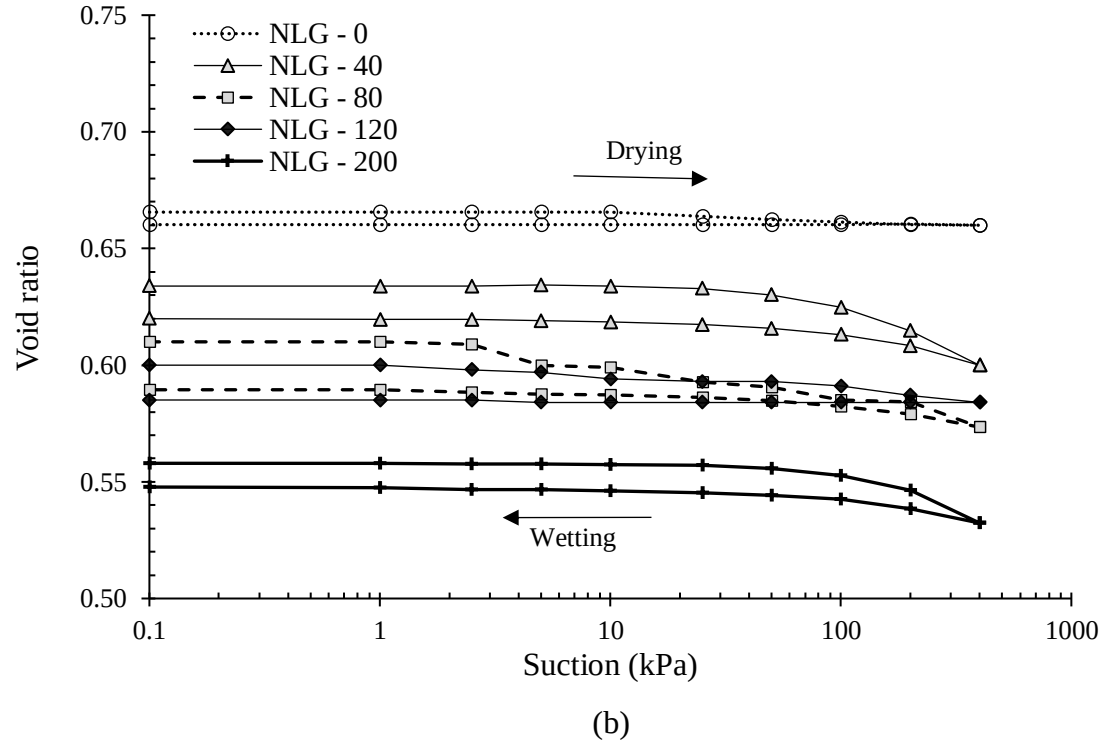

(b)

Figure 7. Variation of void ratio against suction at different net stresses. (a) for NLG; (b) for GLH.

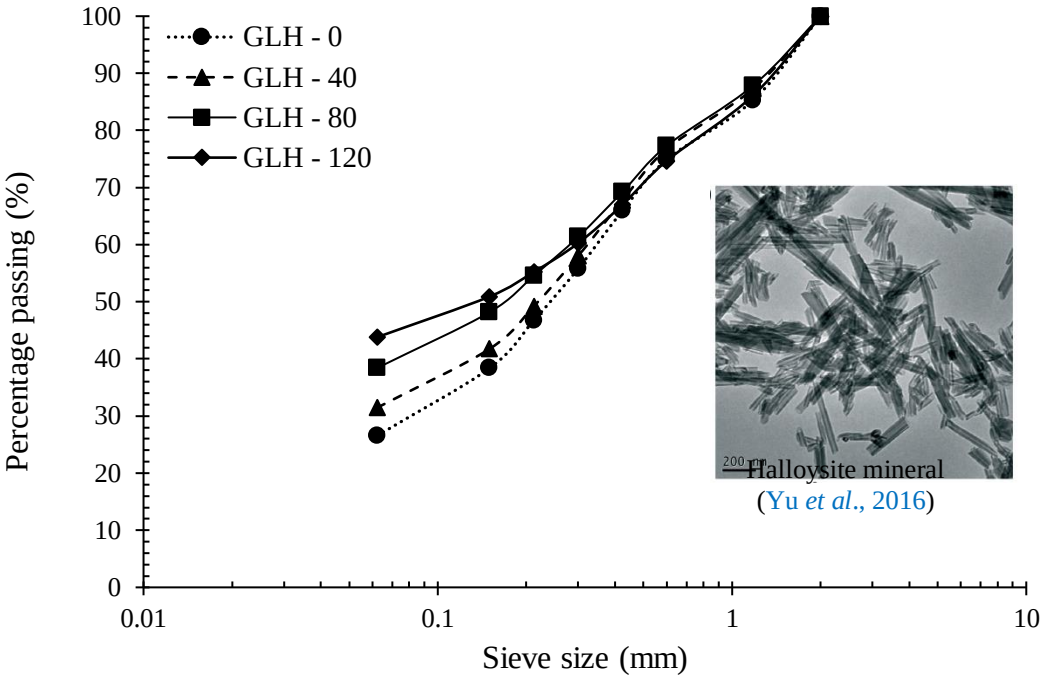

(a)

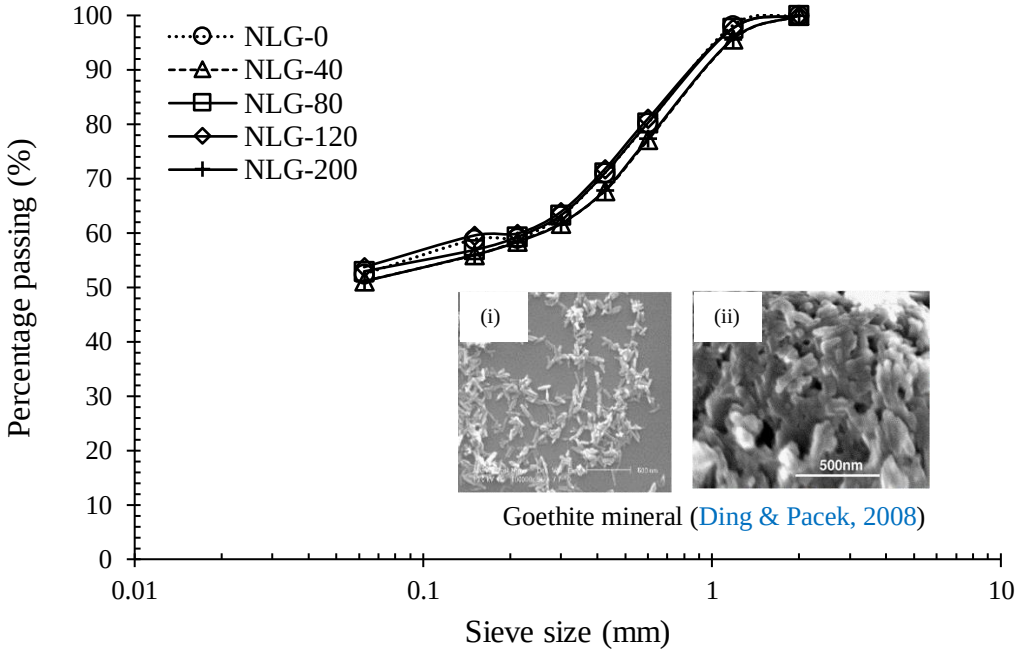

(b)

Figure 8: Influence of stress level on particle size distribution. (a) for GLH; (b) for NLG.

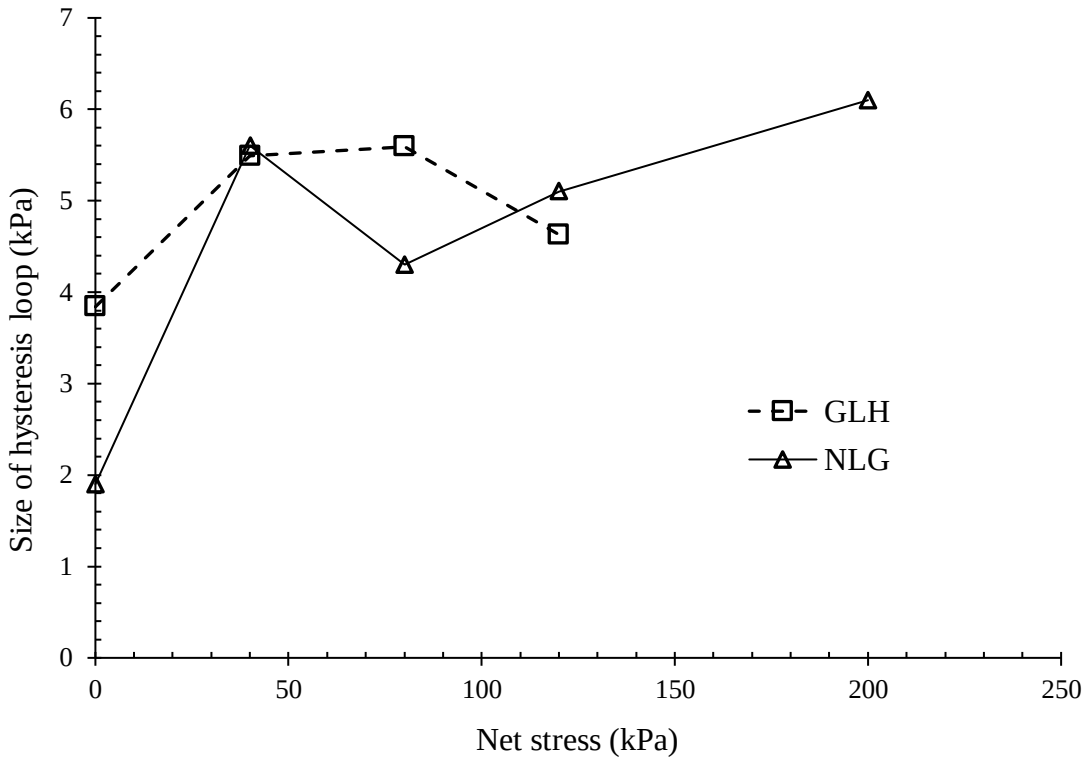

Figure 9: The size of hysteresis loop against net stress.

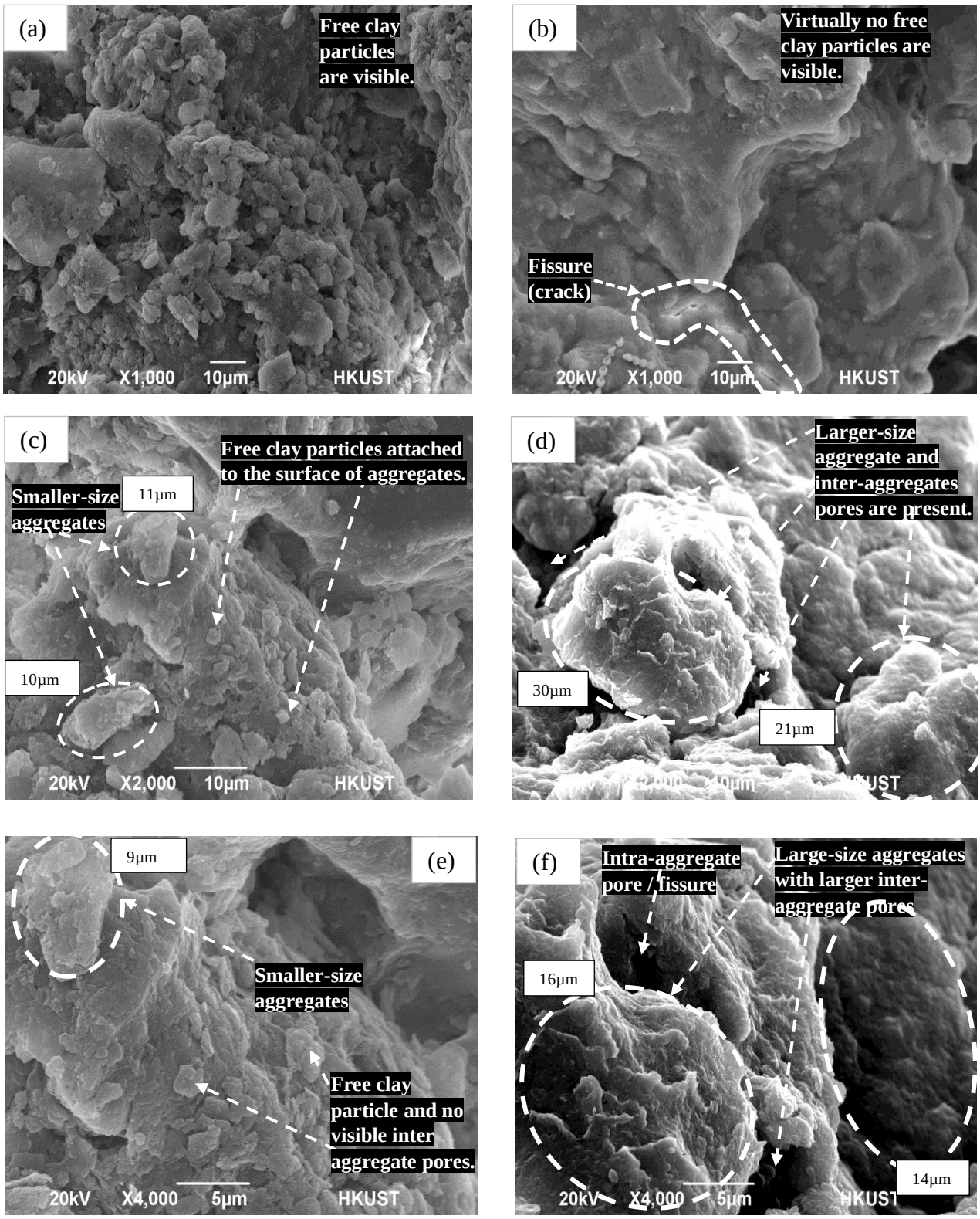

Figure 10: SEM images of the two soils at different magnifications; (a) GLH X 1,000; (b) NLG under X 1,000; (c) GLH X 2,000; (d) NLG under X 2,000; (e) GLH soil under X 4,000; (f) NLG under X 4,000.

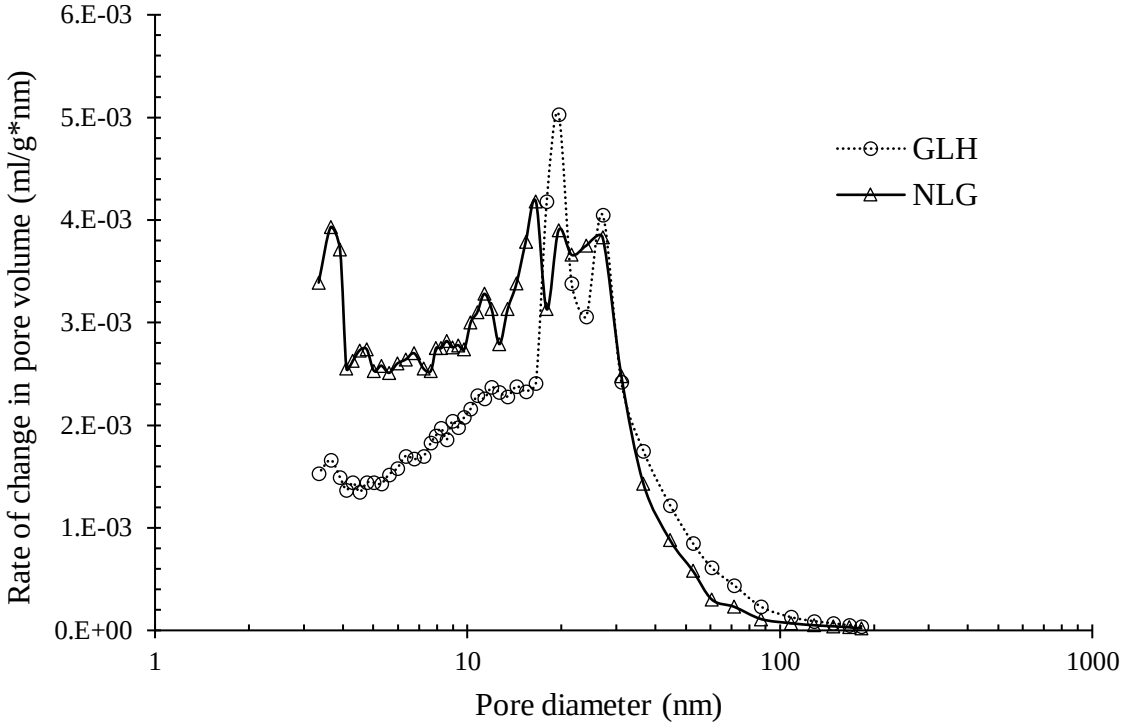

Figure 11. Pore size distribution at nano-scale.